Geomechanics and Engineering, *Vol. 40, No. 5 (2025) 323-338*
https://doi.org/10.12989/gae.2025.40.5.323

Numerical modelling on the behavior of strip shell footings placed on reinforced slopes

Gholamhosein Tavakoli Mehrjardi*, Masoud Khoshnevisan[a] and Elham Sattari[b]

Department of Civil Engineering, Faculty of Engineering, Kharazmi University, Tehran, Iran

(*Received April 20, 2022, Revised February 5, 2025, Accepted February 10, 2025*)

Abstract. Optimal use of construction materials takes center stage in engineering problems so much so that new techniques are daily proposed. Application of shell footings with various geometries are good cases in point in the novel system of foundation engineering. This study aims to present a numerical simulation of laboratory model tests by FLAC 3D software, developing an understanding of the behavior of shell strip footing located at the adjacent of unreinforced and geotextile-reinforced slopes. In this regard, bearing capacity and settlement of the shell foundations by considering contributory factors, notably apex angles, distances of the footings from the crest of the slope namely "edge distance", slope angle, stiffness of the footing core in shell footings, and reinforcement status were studied. The results indicated that the ultimate bearing capacity of foundations increases with decrease of apex angle and increase of footings edge distance. It was also observed that the core in shell footings plays a key role in stress transfer though the foundation depth so that dense soil among the others brought about the highest bearing capacity. At the end, the applicability and interpretation of the obtained results for prototype model were discussed.

Keywords: bearing capacity; numerical modelling; reinforced soils; shell footings; slopes

1. Introduction

Shell foundations are capable of supporting higher vertical loads, better load-settlement characteristics and are economical in terms of material compared with the conventional footings (Shaligram 2011). Due to their many advantages, shell foundations have attracted many researchers from the 70s, worldwide. Iyer and Rao (1970) conducted a series of experimental tests to investigate the bearing capacity of shell foundations and compared the results with their plain counterparts. The results highlighted the importance role of shell foundations in increasing bearing capacity next to flat foundations due to the stiffness and geometry of shell elements. Kurian and Mohan (1981, 1983) reported the contact pressure distribution for various shell shapes. Results were indicative of a non-uniform contact pressure distribution along the shell-soil interface. Moreover, Hanna and Abdel-Rahman (1990) performed experimental and theoretical investigations on triangular shell (folded plate) strip footings in the upright position, resting on sand. They found out that for the same width of footing, a triangular strip footing had higher bearing capacity and better settlement characteristics than its plain counterpart. Additionally, Hanna and Abdel-Rahman (1998) investigated the performance of shell foundations in terms of bearing capacity and settlement. They performed their tests on conical, triangular and pyramidal shell foundations as well as circular, strip and square flat foundations. They noted that shell foundations had better performance than flat foundations and failure surfaces in the former were deeper than the latter. Esmaili and Hataf (2008) studied the ultimate load capacities of conical and pyramidal shell foundations on un-reinforced and reinforced sand by laboratory model tests and numerical analysis. The results were compared with those for circular and square flat foundations. Both the experimental and numerical studies showed that, if shell foundation thickness increases, the behavior of the shell foundation on either reinforced sand or un-reinforced sand gets closer to that of flat foundations. The ultimate load capacity of shell foundations was observed higher than that for counterpart flat foundations. Moreover, El-kady and Badrawi (2017) studied experimental testing and numerical analysis to investigate the ultimate load capacity and settlement variations of folded isolated foundations on sand. The measured and computed total settlements showed that increasing the folding angle more than 30° with the horizontal was not effective in reducing the stresses and consequently the total settlements. It was observed that settlements for the folded isolated footing were much lower than the settlements for the flat bottom footing by about 57%.

Geosynthetics reinforcements have been considered one of the most, if not the most, powerful methods in soil improvements so much so that they are widely used in geotechnical projects (Indraratna *et al*. 2013, Moghadas Tafreshi *et al.* 2015, 2016, Ferreira *et al.* 2016, Tavakoli Mehrjardi *et al*. 2016, 2017, 2019, 2021, Suku *et al.* 2017, Cardile *et al*. 2017). Therefore, using geosynthetics reinforcements beneath the shell foundations is timely and crucial. Shaligram (2011) and Azzam and Nasr (2015) studied the bearing capacity of triangular shell strip footings

*Corresponding author, Associate Professor
E-mail: ghtavakoli@khu.ac.ir
[a]M.S.c
[b]M.S.c

ISSN: 2005-307X (Print), 2092-6219 (Online)

on unreinforced and geotextile-reinforced sand using experimental models. They evaluated the effects of soil compaction and geotextile reinforcement beneath the foundation on the maximum bearing capacity of shell footing. Their studies confirmed increase of bearing capacity of shell footings with decrease in apex angle. Moreover, decrease in bearing capacity was observed due to increase in depth of geotextile layers. Furthermore, their investigations illustrated that the failure wedge of reinforced shell foundation was formed deeper than conventional flat ones.

In the age of cities development, urban sprawl forces the engineers to construct the structures such as buildings and bridge abutments adjacent to slopes. From a geotechnical point of view, bearing capacity of footing may be significantly reduced depending upon the location of the footing from the crest of the slope and the slope angle (Meyerhof 1957, Shields *et al*. 1977, Borthakur *et al*. 1988, Javankhoshdel and Bathurst 2016). This paper seeks to investigate more efficient, yet still reliable backfill underneath of shell footings by using geotextile reinforcements. This is achieved by the use of numerical simulations, using the FLAC 3D computational code, that reproduce reduced-scale plate load tests which have been conducted by Gaffari *et al*. (2021). As a whole, this study in compared with the reduced-scale model tests, exhibited further studies to understand the stress distribution in the backfill beneath the shell footings in comparison with flat footings. Moreover, the interpretation of the obtained result for prototype problems (scale effect), influence of contributory factors such as the core in shell footings, stiffness of shell footing materials, and slope angle, which were not considered in the tests and not easily achievable using experimental models, will be discussed in this paper.

2. Numerical simulation

The numerical simulations were performed using the commercial software FLAC 3D as a three-dimensional explicit finite difference program [FLAC 3D (Itasca 2011)]. The geometry of the model, its calibration, verification and parametric studies are discussed in the following sections.

2.1 Model geometry and boundary conditions

To lay groundwork for verification of the numerical simulations, an experimental study performed by Ghaffari *et al*. (2021) has been used. Fig. 1 shows the schematic representation of the test setup including test box made of a steel frame, having inside dimensions of 1200 mm × 670 mm in plan (1200 mm in length in X direction and 700 mm in width in Z direction) and 400 mm in height (Y direction).

As can be seen in Fig. 1, in reinforced status, two layers of geotextiles namely the first (top) and the second (lower) layers were installed beneath the footing. The burial depth (u), the distance between the layers (h), the length of geotextiles (L) were considered 0.5B (50 mm), 0.7B (70 mm), and 6B (600 mm), respectively in which B is the loading plate's width. Moreover, the angel and height of the slope were 45 degrees and 400 mm, respectively.

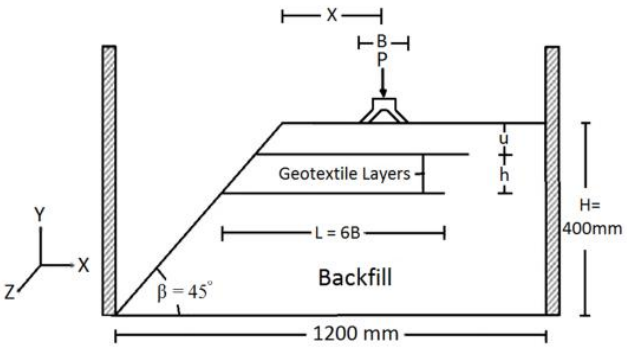

Fig. 1 Schematic representation of the test setup X-Z section (Ghaffari *et al*. 2021).

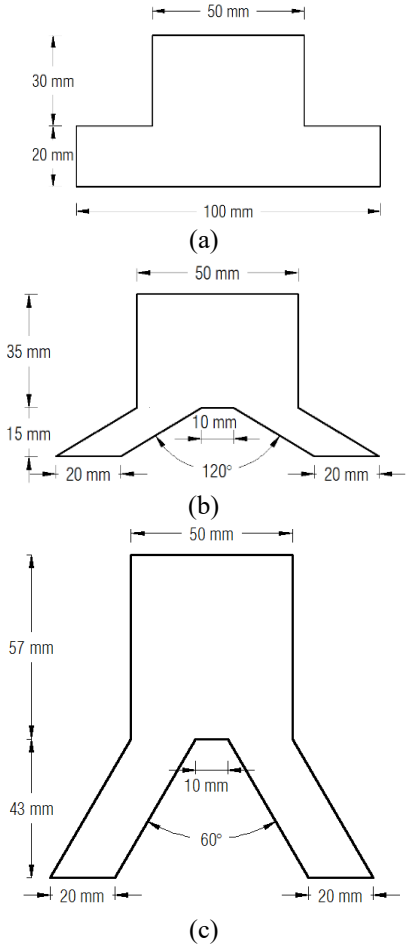

Fig. 2 Geometrical configurations of shell footings with different apex angle; (a) Flat Footing, (b) shell i=120 and (c) shell i=60 (Ghaffari *et al*. 2021)

In the experimental study, the shell strip footings, made of aluminium, with apex angles of 60 and 120 degrees and also, flat strip footing (or shell strip footing with apex angle of 180°) were examined. As can be seen in Fig. 2, the width of all footings was 100 mm. As a whole, the investigated parameters in laboratory tests consisted of the reinforcement and unreinforcement status, the edge distance (distance between the centre of the footings and the crest of the slope, X= 1B, 2B, 3B, 4B), and different apex angles (i= 60°, 120°, 180°). Each test was conducted to study the

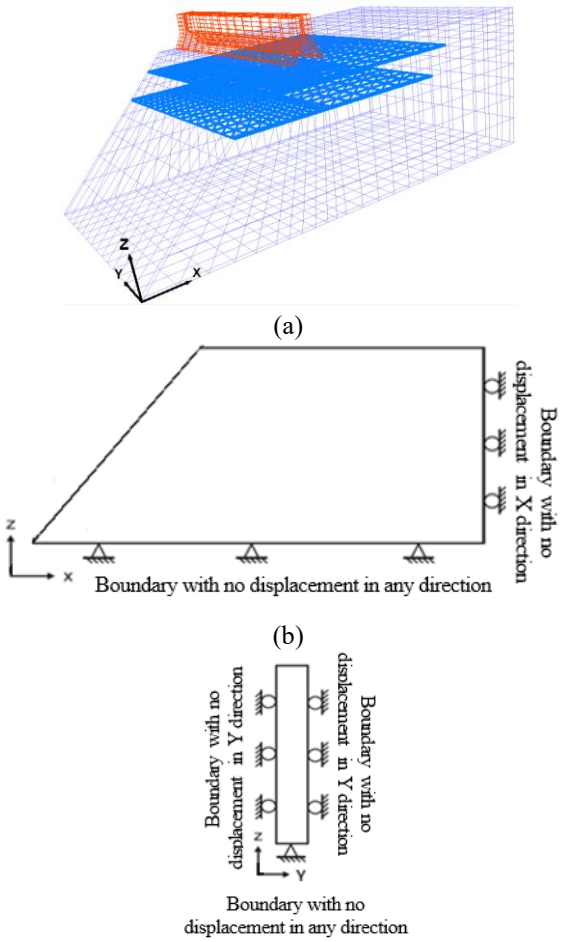

Fig. 3 Simulated model with (a) Geometry of the model; Boundary conditions, (b) X-Z section and (C) Y-Z section

influence of one parameter while the other parameters remained constant. It should be also mentioned that a test of no-slope back fill namely "plane" has been performed to see how far the response of slope backfills in both reinforced and unreinforced conditions are in comparison with that of the plane backfill.

Fig. 3(a) shows the meshed geometry of the slope backfill, geotextile layers and the footing. The domain was divided into 34836 mesh "openings", consisting of brick pattern, connected by 41908 grid points. A relatively fine mesh was used near the slope surface due to stress concentration near the footing. The geotextile layers were simulated by structural element namely "geogrid-element" in FLAC 3D. Due to smooth surface of the footing, to the nature of loading and to the type of embankment used, no interface was considered between the backfill and the footings. Furthermore, the bottom boundary is fixed against movements in all directions; while the vertical boundaries are restricted in the normal direction to its plane and free to move in the vertical direction (see Fig. 3(b)).

2.2 Material properties

In this study, three different materials, including footing, geotextile reinforcement and backfill soil were utilised. The footings were made of Aluminum 6061 and therefore, they were assumed to behave as linear-elastic materials with technical characteristics mentioned in Table 1 in which the mentioned parameters are Young's modulus (E), Poisson ratio (υ), density (ρ) and tensile stress (σ_t) of Aluminum

Table 1 Properties of footing element

Element	Material	E (kPa)	(υ)	ρ (kN/m3)	σ_t(kPa)
Footing	Al 6061	68.9×10^6	0.33	27.10	150×10^3

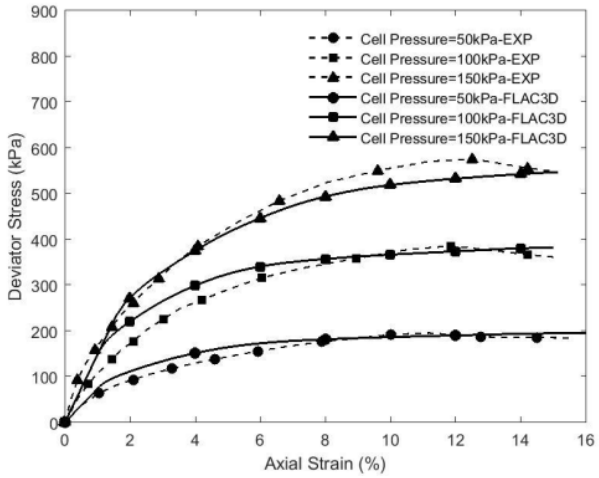

Fig. 4 Comparison of numerical and experimental results of consolidated-drained (CD) triaxial tests under different confining pressures (50, 100, and 150 kPa)

Since, high Strength Polyester Woven Geotextiles (TFI 3100) were used in experimental study; therefore, the element type "geogrid" was used in the numerical analysis. Geogrid structural elements are three-nodes flat elements that resist tension forces in the plane but do not resist bending loading. The truth is that the results of pull-out test are required to appropriately define the interfacial properties of geotextile and backfill soil. Due to the absence of this data, the required parameters in Table 2, notably Young's modulus (E), Poisson ratio (υ), thickness (t), coupling spring cohesion (cs-scoh), coupling spring friction (cs-sfric), and coupling spring stiffness (cs-sk) were determined by back-analysis.

To simulate the response of backfill under applied stresses, the strain-softening Mohr-Coulomb failure criterion was used. The values for each of the model parameters were obtained by using triaxial tests from Ghaffari *et al*. (2021) were performed on the original soil materials under different confining pressures (50, 100, and 150 kPa). Then, triaxial tests were simulated and modeled with FLAC3D and the input parameters were calibrated and modified until the results of the numerical analyses closely matched those obtained from experimental model as shown in Fig. 4. Table 3 represents values of the calibrated parameters, including Young's modulus (E), Poisson ratio (υ), density (ρ), cohesion (c), friction angle (ϕ), dilation angle (ψ) and tensile stress (σ_t).

Table 2 Technical properties of geotextile element used in the numerical analysis

Element	Geotextile properties			Geotextile interface properties		
	E (GPa)	(υ)	t (mm)	cs-scoh (kPa)	cs-sfric (degree)	cs-sk (kPa)
Geotextile	26	0.33	3	2	41	50×10^3

Table 3 Properties of embankment element used in the numerical analysis

Element	Material	E (kPa)	(υ)	ρ (kN/m3)	ϕ (◦)	c (kPa)	ψ (◦)	σ_t(kPa)
Embankment	sand (SP)	35000	0.3	17.72	41°	2	11°	2.3

Table 4 Cohesion, friction, and dilation changes in terms of the shear strain alterations used in the numerical analysis

shear strain (%)	0	35×10^{-3}	45×10^{-3}	55×10^{-3}	60×10^{-3}	1
Cohesion (kPa)	2	1.85	1.7	1.6	1.5	1.5
Friction angle, ϕ (◦)	41	39	37	36	35	34
Dilation angle, ψ (◦)	11	9	7	6	5	4

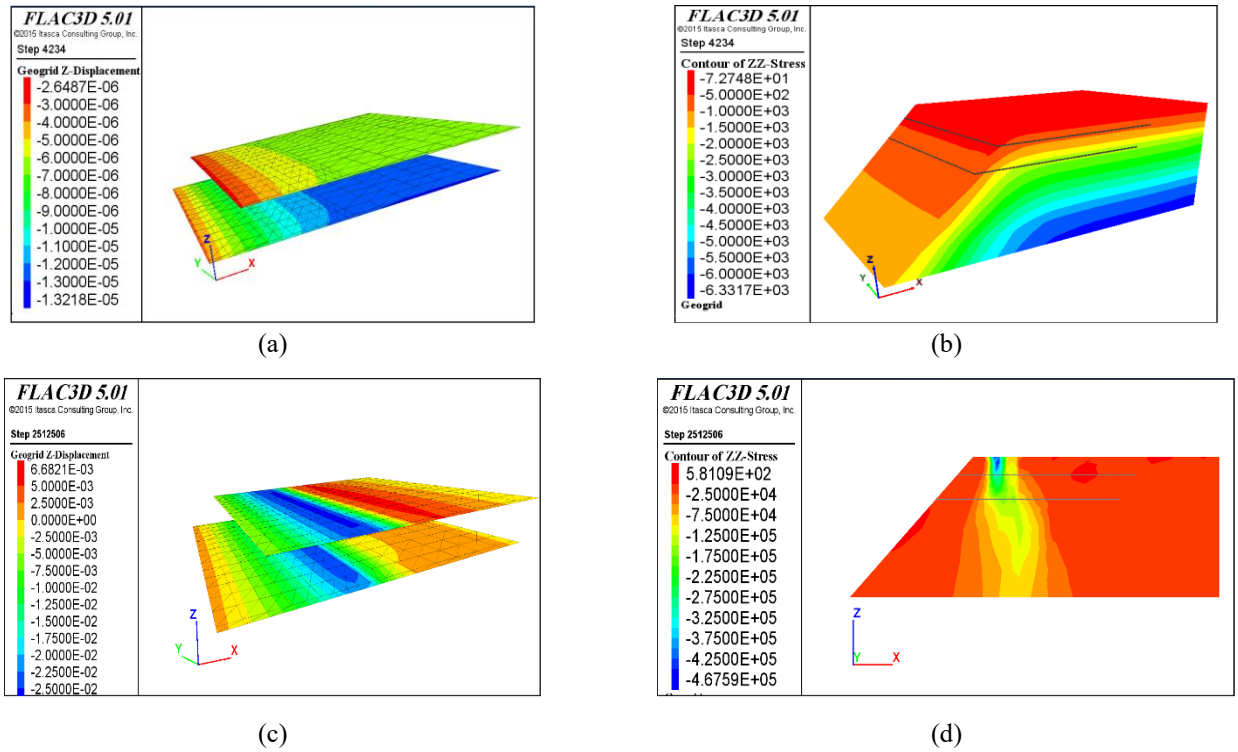

Fig. 5 Model verification for shell footing with apex angle of 60° located at X=1B (a, b) vertical stress and geotextiles tensile deformation under staged construction, (c, d) vertical stress and geotextiles tensile deformation under surface loading at the end of analysis

To simulate the softening performance of backfill after the peak stress, according to Table 4, the shear strength parameters, notably cohesion, friction angle, and dilation angle were reduced with increment of shear strain, correspondingly.

2.3 Verification of the model

To verify the numerical model, the slope backfill was simulated by considering staged construction performed in the tests, establishing the in-situ stresses through the soil medium. Figs. 5(a) and 5(b) depicts vertical stress in the reinforced slope propagated due to gravitational body forces and the corresponding tensile deformations in the geotextile layers.

Then, the settlements induced in the backfill set to zero so as to have the settlements as of plate loading stage. Finally, in order to simulate surface loading on the backfill,

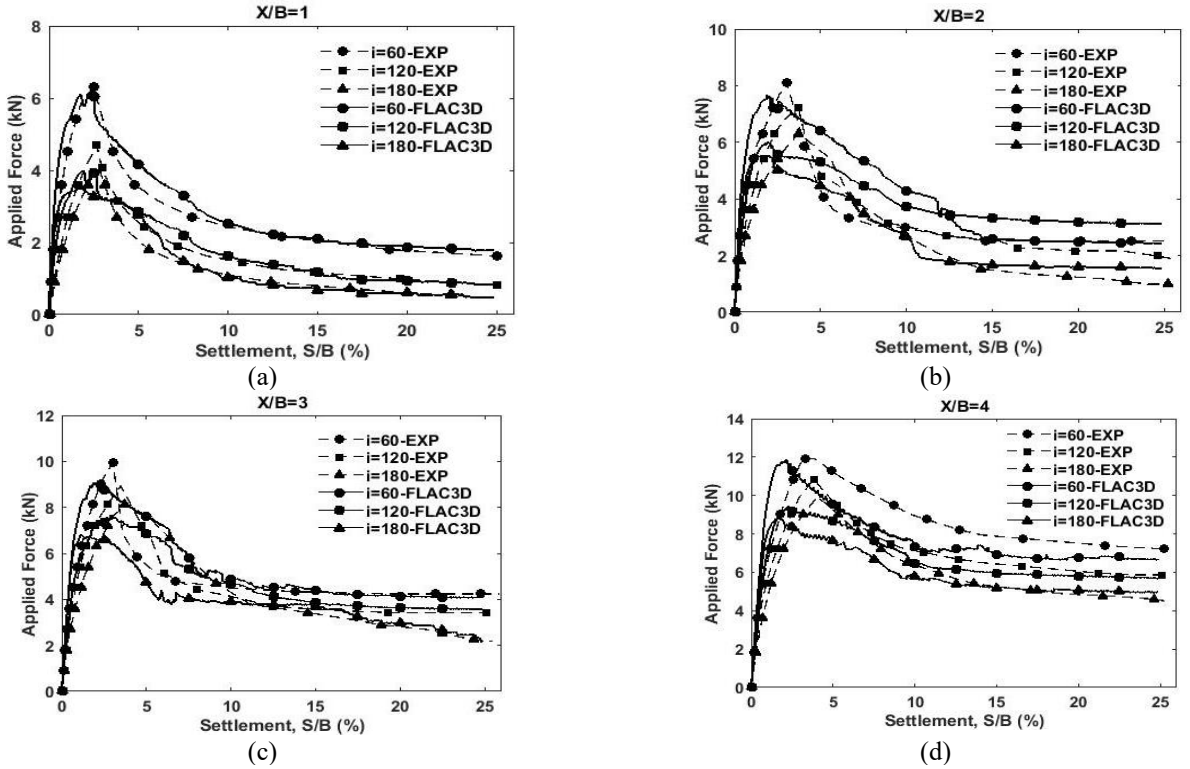

Fig. 6 Response of the footings situated at unreinforced slope with edge distance of (a) x=100 mm, (b) x=200 mm, (c) x=300 mm, and (d) x=400 mm

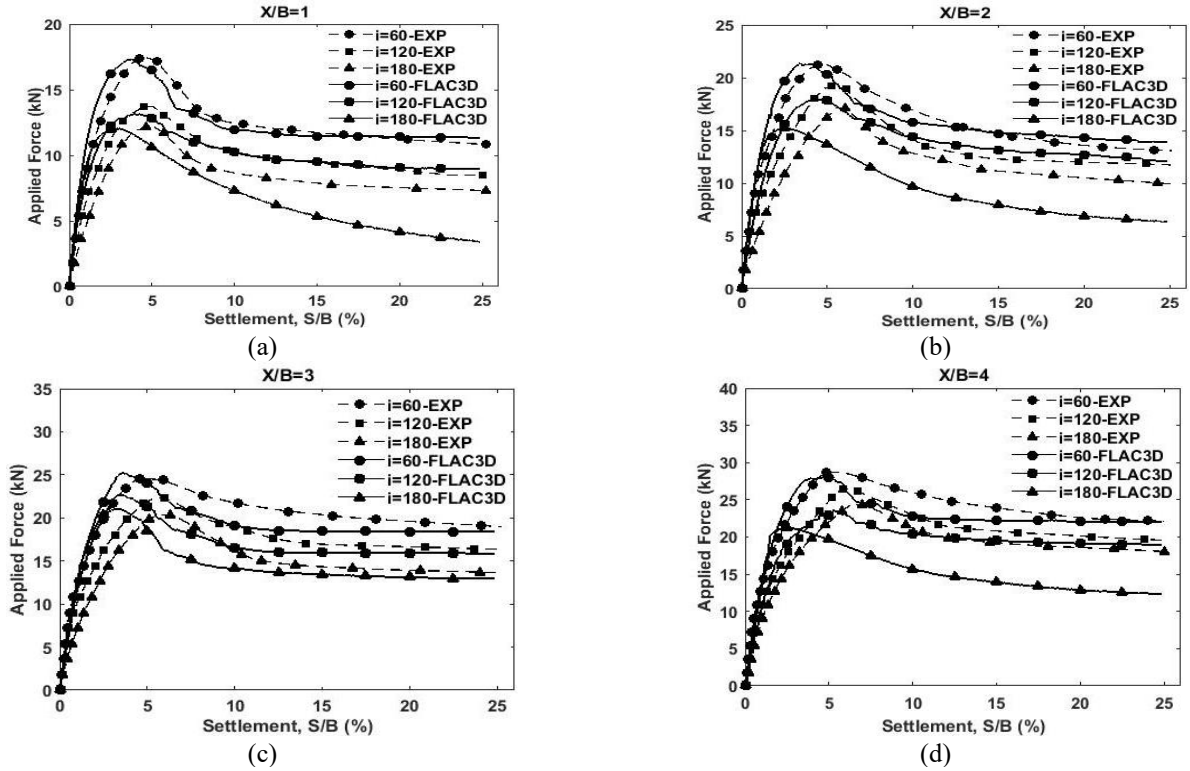

Fig. 7 Response of the footings situated at reinforced slope with edge distance of (a) x=100 mm, (b) x=200 mm, (c) x=300 mm, and (d) x=400 mm

a constant grid-point velocity of 1e-8 m/s with 2500000 steps was applied, reaching 25 mm settlement. Figs. 5(c) and 5(d) represents the vertical stress due to surface loading and tensile deformations in the geotextile layers at the end of analysis for shell footing with apex angles of 60° located at edge distance x=1B.

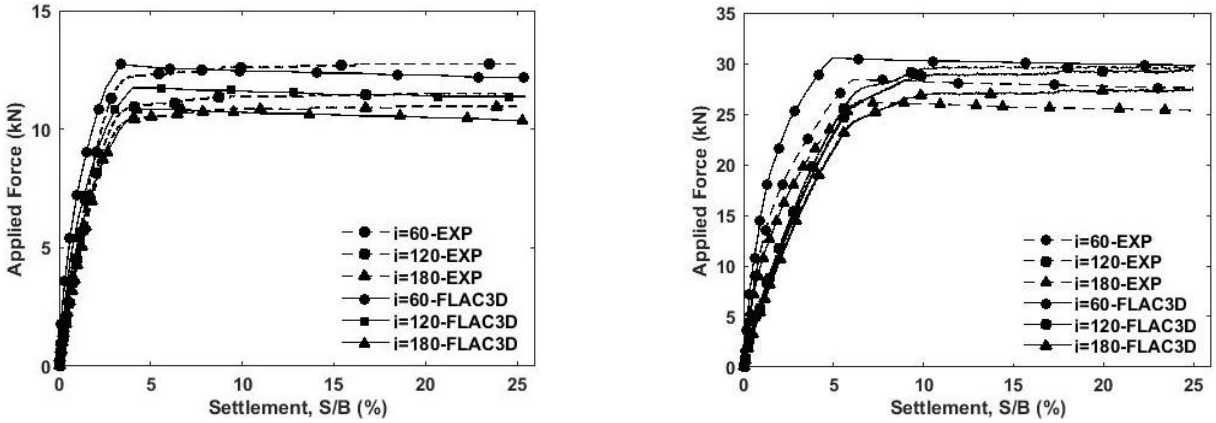

Fig. 8 Response of the footings in "plane" status for (a) unreinforced and (b) reinforced backfill

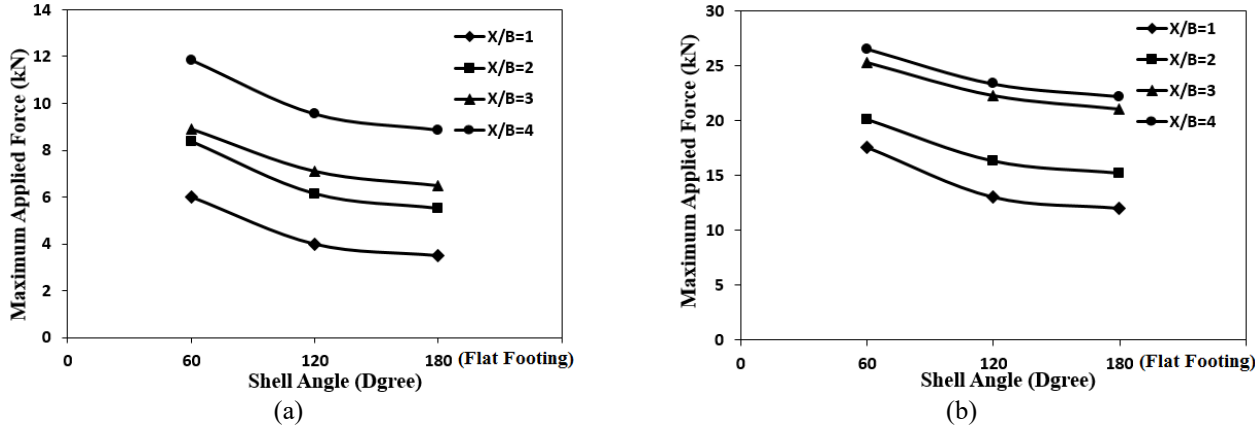

Fig. 9 The bearing capacity changes against different edge distances for; (a) unreinforced, and (b) reinforced, slopes

Figs. 6 and 7 compare the load-settlement curves obtained from the numerical analysis and the laboratory tests for different footing edge distances (x) and variable apex angle (i) in both unreinforced and reinforced conditions.

Moreover, Fig. 8 compares the load-settlement curves obtained from the numerical analysis and laboratory tests for the footings with different apex angle (i) in the "plane" status (no slope) backfill for both unreinforced and reinforced conditions.

In general, the current numerical modelling could appropriately simulate the experimental models. In effect, although the peak bearing loads acquired in the numerical modelling were slightly different in comparison with those in the experimental results (the average differences were about 11% and 7% for unreinforced and reinforced conditions, respectively), indeed the softening behavior of the slope after the peak load could successfully simulated so that the trend of variations were in good agreement with experimental results.

3. Parametric analysis

There are a few key factors affecting the response of shell footings situated on the unreinforced and reinforced slopes. Apex angle, edge distance, material of the footings, and the density of filling core are just good cases in point. In this section, the roles of these contributory factors on the slope performance in both unreinforced and reinforced conditions are discussed. Moreover, the failure mechanisms, taking a centre stage in exploring the shell footing response, are investigated.

3.1 Apex angle

Fig. 9 shows the influence of apex angle on the maximum bearing load tolerated by different types of shell footings in both unreinforced and reinforced conditions. It can be clearly seen that with decreasing the apex angle from 180° to 60°, the bearing capacity climbed drastically irrespective of reinforcement status and edge distance.

Also, it is obvious that the maximum applied load in reinforced tests were larger than that in unreinforced condition. According to Fig. 10, although the widths of all footings were kept constant, arguably the contact area of the shell footing with apex angle 60° with soil through the core was larger in comparison with the other types of footings, leading to propagation of the lower vertical stress in the backfill. To show a clear picture of this phenomenon, the vertical stresses propagated at the level of 0.05 m beneath the footings for both unreinforced and reinforced slopes are illustrated in Fig. 11. Obviously, regardless of reinforcement status, the vertical stress level in shell

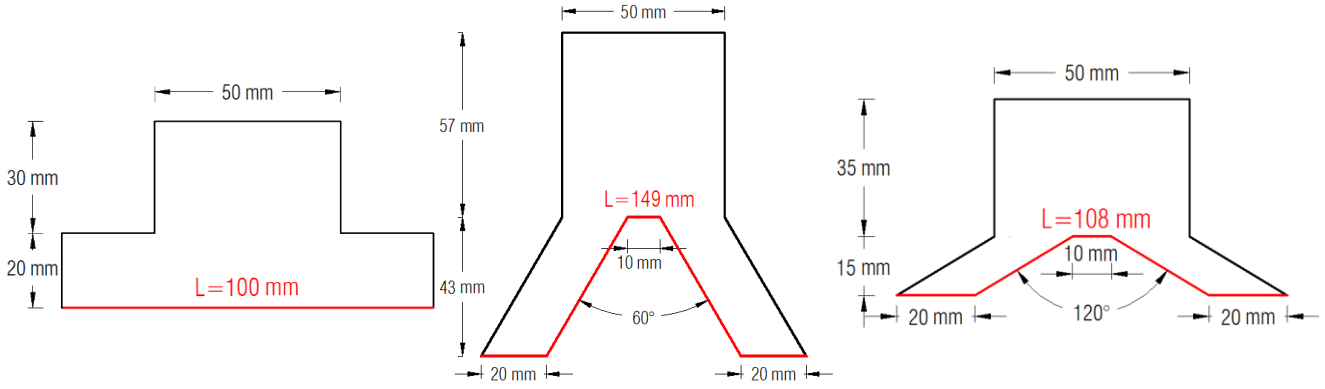

(a) (b) (c)

Fig. 10 Comparison of contact surface for (a) Flat Footing, (b) shell i=60, and (c) shell i=120

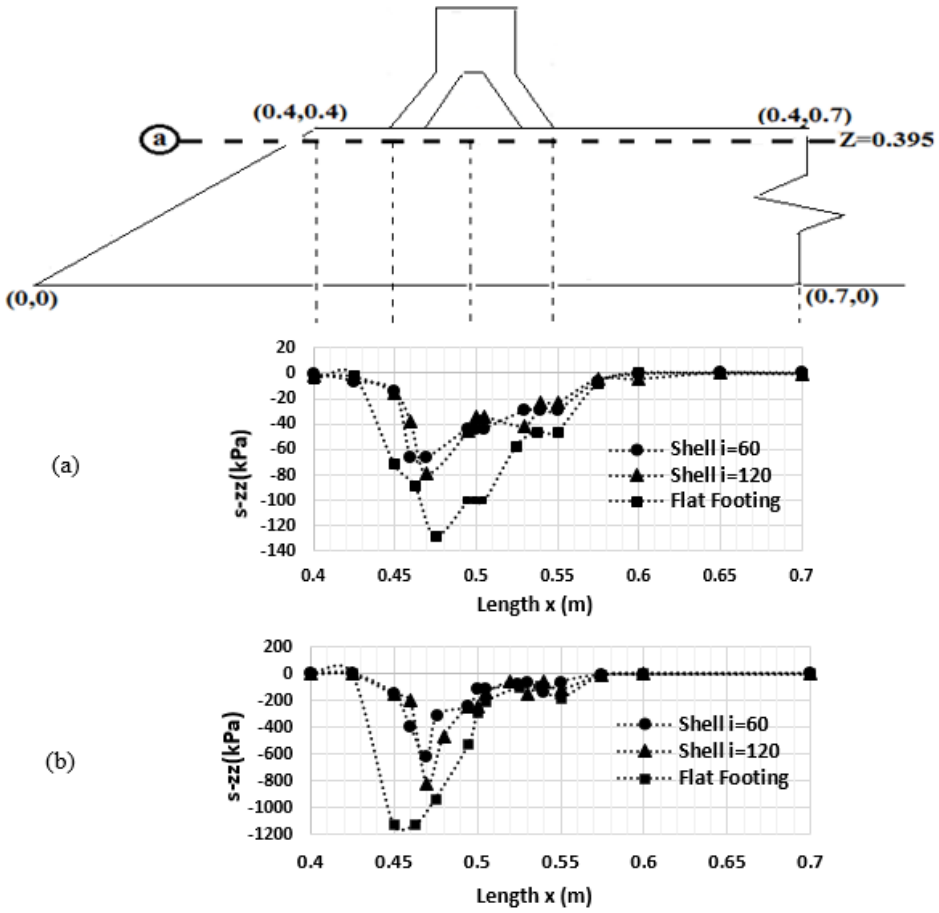

Fig. 11 Comparison of the normal stresses distribution (in Z direction) for shell and flat footings at the level of 0.05 m beneath the footings for (a) unreinforced, and (b) reinforced slopes.

foundations is about 50% to 75% of that in flat foundation. In effect, the core plays a key role in stress reduction.

3.2 Edge distance

Looked at from geotechnical point of view, it is important to define a safe edge distance in which the bearing capacity of foundation is equal to the plane status (no-slope backfill). To assess the sensitivity of bearing capacity of the footings situated at the slope backfill, Fig. 12 is presented. In this Fig., Improvement Factor (IF) is defined as the ratio of the bearing capacity of footings in unreinforced or reinforced "slope" status $(q_u)_i$ to that in the unreinforced "plane" status $(q_u)_p$. In fact, IF≥1 (illustrated with dashed line in Fig. 12) declares that the bearing capacity of footing located at the slope surface was not only out of the shear failure zone occurred in the common slope backfills, but also enhanced due to providing safe edge

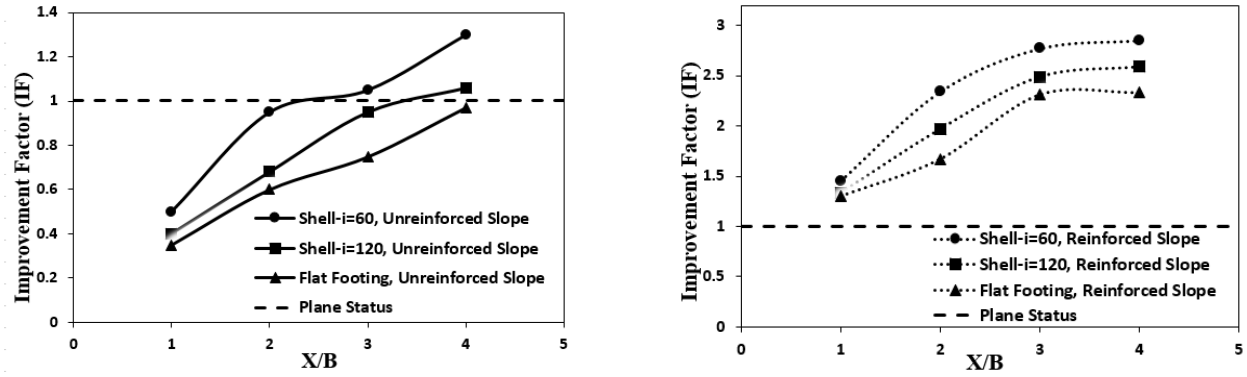

(a) (b)

Fig. 12 Variations of Improvement Factor vs edge distance for all footings in (a) unreinforced slopes, and (b) reinforced slopes

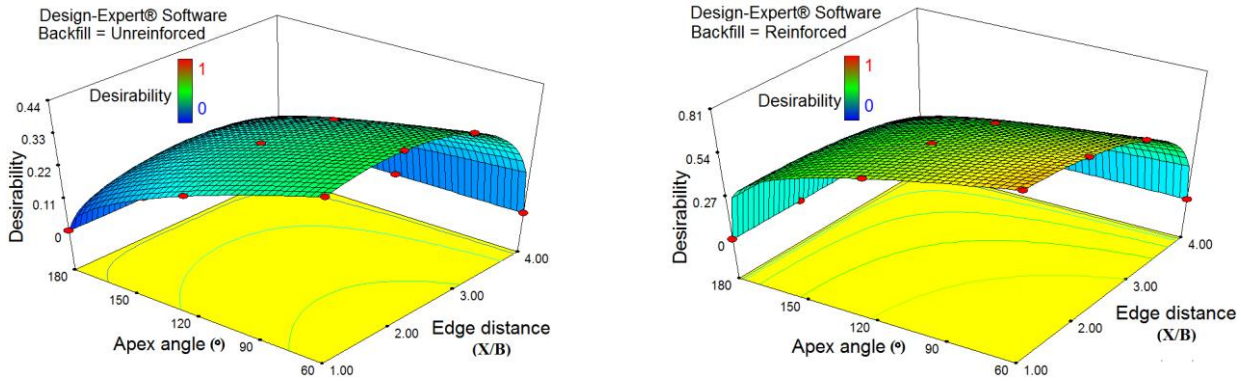

(a) (b)

Fig. 13 The influence of apex angle and edge distance together to get the optimum bearing load tolerated by different types of shell footings in (a) unreinforced slopes, and (b) reinforced slopes

distance, footing shape, or reinforcement layers.

As can be seen in Fig. 12(a), in unreinforced slope, an increase of edge distance brought about the better performance of footing so much so that the larger edge distance, the higher improvement factor is obtained. Broadly speaking, the safe edge distance for shell footing with apex angle of 60° is 2B, while that for flat footing is about 4B. This confirms that shell footings over the slope surface are more reliable in contrast with conventional flat footings. Furthermore, according to Fig. 12(b), the presence of reinforcement layers could successfully improve the slope stability of the backfill against applied stress for all kinds of footings and regardless of edge distance, acquiring IF>1. It is worth bearing in mind that in reinforced conditions, irrespective of footing type, IF remained unchanged over the edge distance of 3B. Although increasing the edge distance enhances the chance of utilizing shear strength planes against footing penetration, indeed it causes a reduction in pull-out resistance of reinforcement layers, making the IF stayed constant over a specified edge distance. In the line with this finding, Tavakoli Mehrjardi *et al*. (2016) found out that for reinforcement length of 6B, the "Improvement Factor" plateaued beyond the edge distance of 2B.

To provide a logical relationship between apex angle and edge distance together on the maximum bearing load tolerated by different types of shell footings in both unreinforced and reinforced conditions, results are analysed using Design Expert software v7.0.0 with significant control parameters and 95% confidence. Final Equations for bearing capacity of foundations (P, kN) in terms of edge distance (X, m) and apex angle (i, degree) are according to Eqs. (1) and (2) for unreinforced and reinforced statuses, respectively. It should be mentioned that R2 of both equations were 0.99.

$$P = 5.33 + 1.82\,X - 0.02\,i \quad (1)$$

$$P = 17.07 + 3.43\,X - 0.05\,i \quad (2)$$

The optimization feature of the software uses a function namely "Desirability" to calculate the optimum operating parameters. In effect, "Desirability" is an objective function that ranges from zero outside of the limits to one at the goal. Therefore, the numerical optimization finds a point that maximizes the desirability function. For this purpose, it is tried to find a combination of edge distance and apex angles

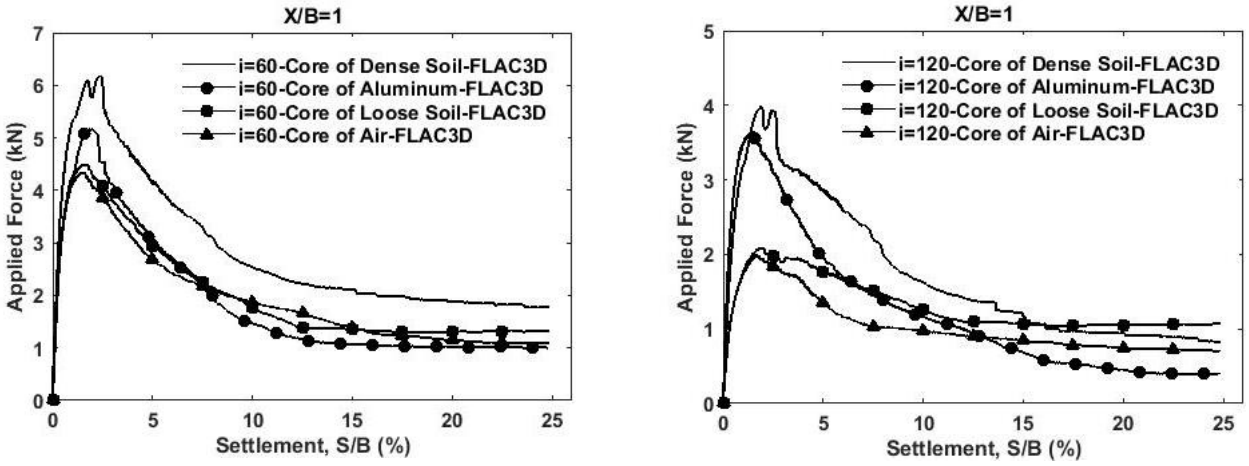

(a) (b)

Fig. 14 Load-settlement curves for shell footings located at unreinforced slopes, with edge distance x=1B, influenced by four different core materials; (a) i=60° and (b) i=120°.

Table 5 Technical properties of materials substituted in the footings' core

Material	E (kPa)	(υ)	ρ (kN/m3)	ϕ (◦)	c (kPa)	ψ (◦)	σ_t(kPa)
Aluminum 6061	68.9×10^6	0.33	27.10	-	-	-	150×10^3
Dense Soil	35000	0.3	17.72	41°	2	11°	2.3
Loose Soil	20000	0.25	17.10	33°	2	3°	3.08

of the foundations in order to achieve the least ultimate bearing capacity which reflected IF>1. Fig. 13 plots 3D surface of "Desirability" versus the input parameters for both unreinforced and reinforced conditions. As can be seen, in unreinforced slopes, the most optimal edge distance and apex angle were 1.8 and 60°, respectively. In reinforced slope, these values are 1 and 60°, reflecting the highest value of "Desirability".

3.3 Substituting material in the core

Practically, it seems that the stiffness of core material in shell footings can play a role in the stress distribution from the footing structure to the backfill medium. To investigate the impact of this crucial factor, different types of materials, including Aluminum, loose soil, dense soil, and air were substituted in the footing core. Table 5 tabulates the technical characteristics of the mentioned materials. It should be noted that null elements were applied to define "air" for footing core.

Fig. 14 shows the load-settlement curves for shell footings with apex angles of 60° and 120° located at unreinforced slopes influenced by four different core materials. As a whole, regardless of apex angle, shell's core made of dense soil obtained the highest bearing capacity among the other materials. Moreover, erecting the shell footings with no material (air) caused stress concentration beneath the footings bases which, in turn, gave rise to the weakest response of the foundations.

Kurian (1994) conducted an experimental study of the shell footing without core. It was noticed that the mechanism of failure was due to the concentration of the soil reactions at the edges. The reduction in ultimate strength under this condition is a clear indication of necessity for ensuring full contact between the footing and the soil in order to prevent premature failures of shell footings.

The sensitivity of foundation response to core materials stems from the stress distribution and shear strains produced in the backfill, especially beneath the footing. Fig. 15 compares the shear strain levels in the foundations for different types of core material. Interestingly, it can be observed that the value of shear strain beneath the shell footings were around 0.9, 1, and 1.35 when the core materials were dense soil, Aluminium, and air, respectively which is the same order in the foundations' response. In effect, the more shear strain, the lower bearing capacity is obtained. Therefore, it is recommended that the soil core in shell footings should comprise dense soil.

3.4 Slope angle

From a practical point of view, constructing steeper slope backfill delivers a multitude benefits for the road clients, especially when the addition land is not available for road widening. To assess the implication of slope inclination on the bearing capacity of shell footings, a pretty chunk of analysis, encompassing variation of slope angles and footing types were carried out. Fig. 16 depicts some of the obtained results for shell footings with apex angles of 60° in both reinforced and unreinforced conditions for different slope angles. As a general trend, increasing the

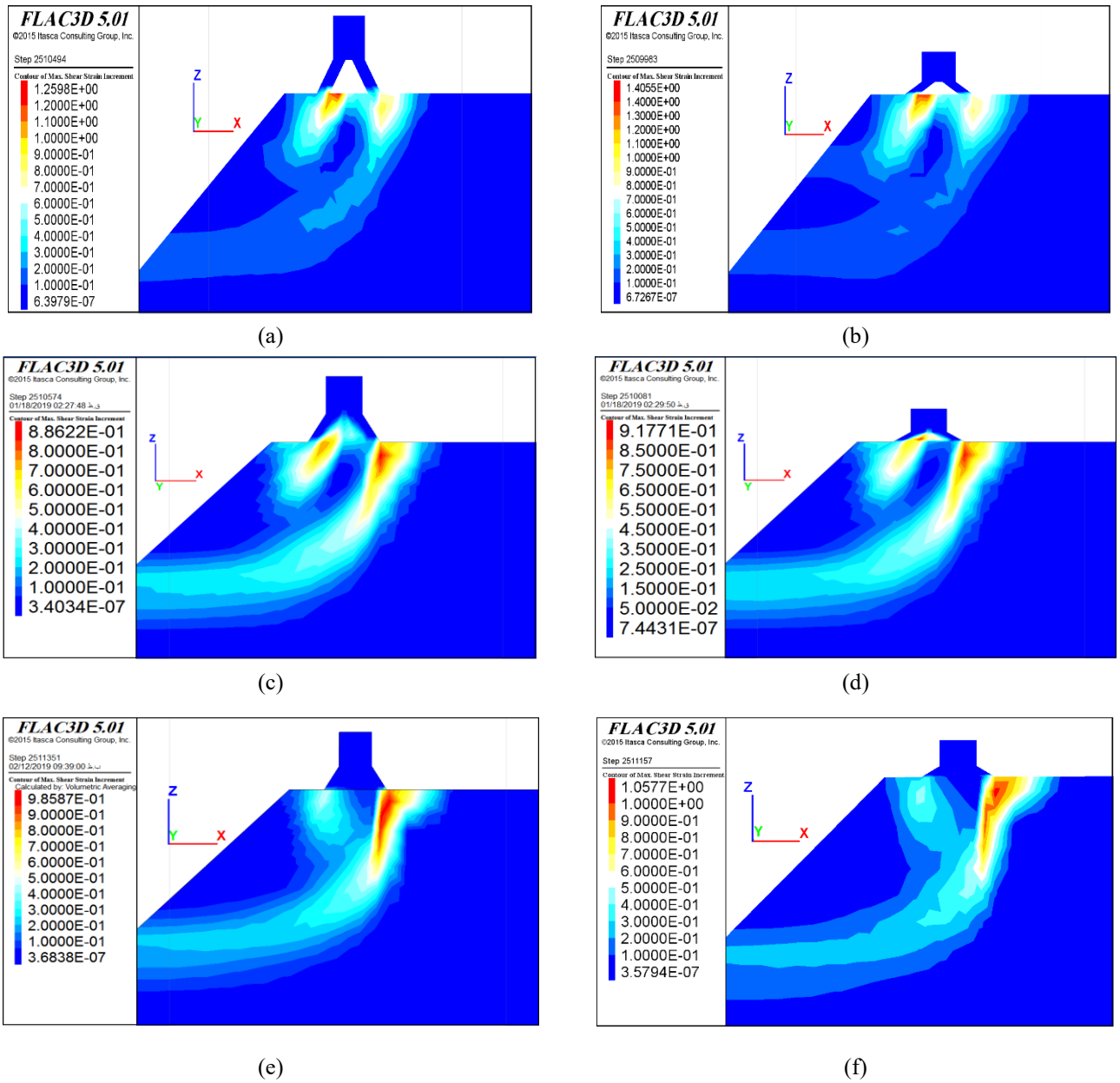

Fig. 15 Shear strain contours for shell footings located at unreinforced slopes, with edge distance x=1B, when the core materials are (a, b) air, (c, d) Dense soil, (e, f) Aluminum (the left side for i=120° and the right side for i=60°)

slope angle makes the bearing capacity of all footings reduced in that a part of shear strength, mobilizing through the shear plane, got vanished. Since, in some projects, the clients are obliged to construct road embankments with steep slope, therefore footing selection and also, using reinforcement elements would be crucial alternatives, tackling the stability difficulties.

In this regard, Table 6 intends to present the improvement factors as well as ultimate bearing capacity for different slope angles, different apex angles of footings at edge distance X=1B in both unreinforced and unreinforced statuses.

According to Table 6, irrespective of reinforcement conditions, the bearing capacity of foundation situated at slope backfill reduced drastically in comparison with plane backfill. Moreover, Improvement Factor for shell footing with apex angle 60° is greater than one in all slope backfills. Efforts have been applied to find a combination of slope angles and apex angles of the foundations in order to achieve the least ultimate bearing capacity which reflected IF>1. Fig. 17 plots 3D surface of "Desirability" versus the input parameters for both unreinforced and reinforced conditions. As can be seen, in unreinforced slopes, the most optimal slop angle and apex angle were 39° and 60°, respectively. In reinforced slope, these values are 50° and 60°, reflecting the highest value of "Desirability".

4. Failure mechanisms

Fig. 19 shows the shear strain contours as well as displacement vectors for all kinds of footings in both

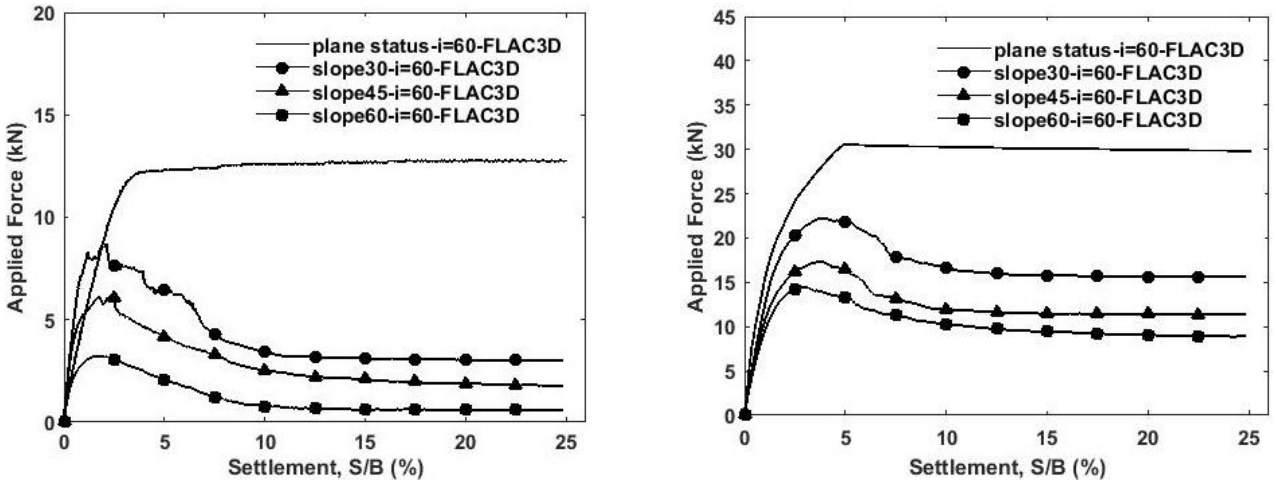

Fig. 16 Response of the shell footings with apex angle of 60° at edge distance X=1B for slope angles of 30°, 45°, 60°, and plane backfill under the applied force for (a) unreinforced, and (b) reinforced embankment

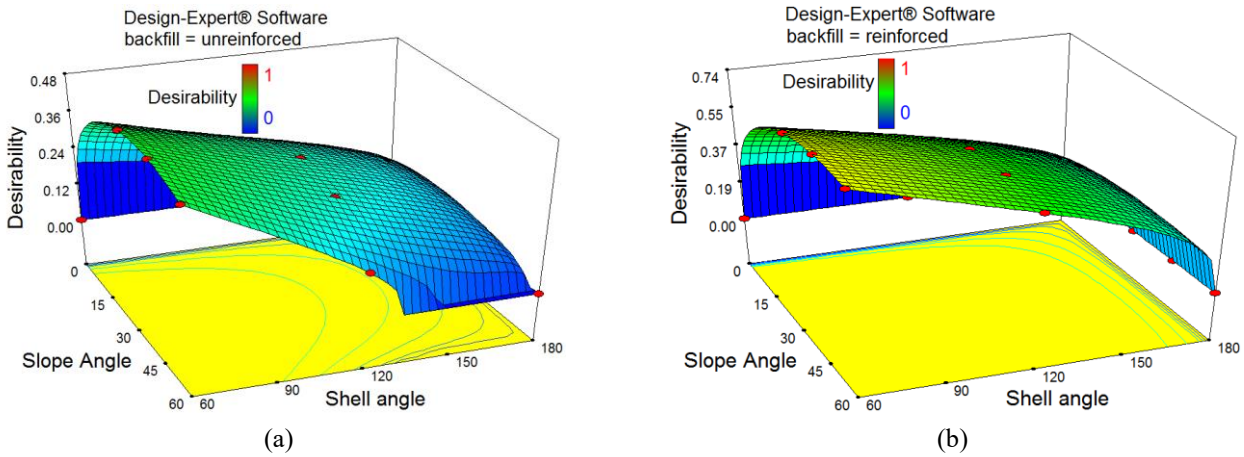

Fig. 17 The influence of apex angle and slope angle together to get the optimum bearing load tolerated by different types of shell footings in (a) unreinforced slopes, and (b) reinforced slopes

Table 6 Ultimate load capacity with Improvement Factor (IF) of each footing with edge distance x=1B in unreinforced or reinforced status

	Slope angle	Maximum Applied Force (kN)			Improvement Factor (IF)		
		i=180°	i=120°	i=60°	i=180°	i=120°	i=60°
Unreinforced Backfill	Plane	9.08	10.39	12.80	1	1	1
	30°	5.56	6.44	8.72	0.61	0.62	0.68
	45°	3.34	4.13	6.28	0.36	0.40	0.49
	60°	2.02	2.6	3.24	0.22	0.25	0.25
Reinforced Backfill	Plane	27.5	28.09	32.03	3.02	2.70	2.50
	30°	16.68	18.21	22.67	1.83	1.75	1.77
	45°	11.86	13.85	17.56	1.30	1.33	1.38
	60°	8.56	9.86	14.58	0.94	0.95	1.14

unreinforced and unreinforced states, specifically at X=1B. Clearly, the overarching value of reinforcement roles in expanding the shear planes from the slope body to its toe cannot be overstressed, enhancing the slope stability. In effect, reinforcement layers could successfully utilize its anchoring length behind the shear plane. It is worth bearing

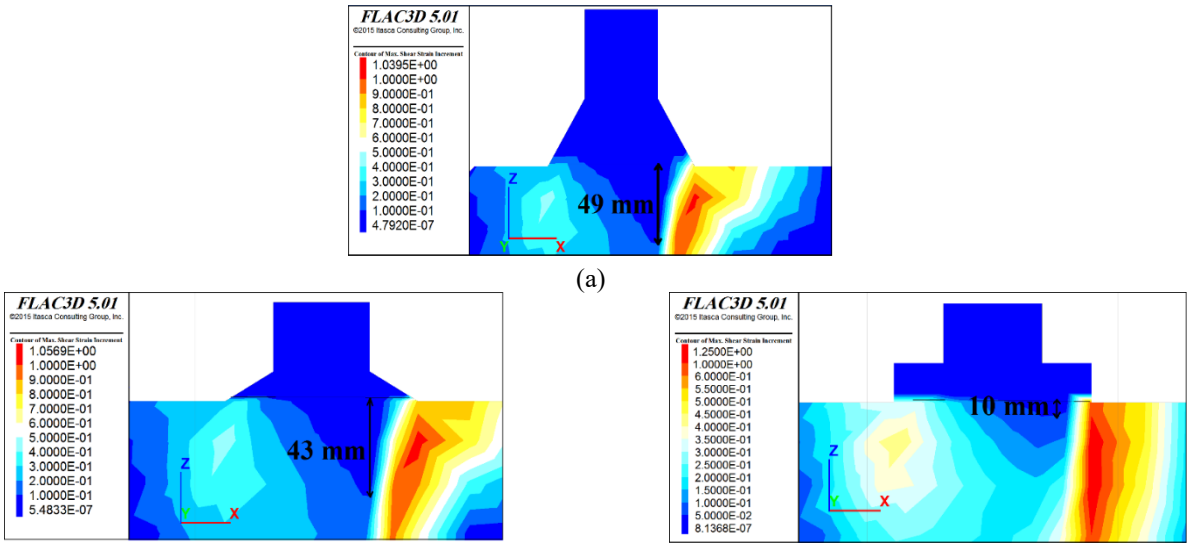

Fig. 18 Shear strain contours as well as failure wedges beneath shell footings of (a) i=60°, (b) i=120°, and (c) i=180° in unreinforced slopes at edge distance 1B

in mind that this effectiveness was more highlighted in the backfill beneath the shell footings in comparison with flat footing. As can be seen, irrespective of the reinforcement conditions, the bearing capacity of flat footings were smaller owing to the fact that the shear strains, propagated beneath the footing, were larger which it confirms the lower efficiency of these footings in contrast with shell footings.

Fig. 18 compares the failure wedge beneath the footings based on the shear strain distribution in slope backfill for all types of footing. According to the results obtained from Ghaffari *et al.* (2021), The visual inspection shows that the wedge angle of the failure surface is increased by decreasing the apex angle, which indicates that the model response is reasonable and it is a good match compared to the failure wedge beneath the footings.

From a geotechnical point of view, failure wedge can be distinguished as a rigid area, experiencing very low shear strain, with a displacement equal to the footing movement. In this regard, it can be clearly seen that the depth of the failure wedge for shell footings with apex angle of 60°, 120° and 180° were about 0.5B, 0.4B, and 0.1B, respectively.

As shown in Fig. 18, more passive forces were provided against the footing penetration, bringing about higher bearing capacity for this kind of footing. It should be mentioned that the small value of failure wedge depth was because of location at the slope surface. Hanna and Abdel-Rahman (1998) monitored the movement of the sand particles beneath triangular shell footings. The results deduced that the rupture surfaces for the shell footings were deeper than those for the flat one which, in turn, led to the increase in the ultimate bearing capacity of the shell footings.

Another way of illustration is comparing the vertical displacements at the ground surface and right side of the footings. As can be seen in Fig. 20, the shell footing with i=60° had the highest heaving which it means that the state of plastic equilibrium is fully developed throughout the soil above the failure wedge and shear failure mode was more similar to general shear failure.

5. Scale effect

Tavakoli Mehrjardi *et al.* (2016) stated that the major physical parameters influencing the response of geogrid-reinforced slope systems can be summarized as: $B.X.u.h.\theta.L.D_r.D_{50}.\phi.c.\gamma.\upsilon.E_{soil}.E_{geo}.b$; where θ is the slope, D_r is relative density of slope's embankment, $\phi.c.\gamma.\upsilon$ and E_{soil} are internal friction angle, cohesion, unit weight, Poisson's ratio and secant elastic modulus of the backfill material, respectively and finally, E_{geo} and b are secant elastic modulus and aperture size of geogrids, respectively. Other parameters have been defined previously. The function (f) governing the geogrid reinforced slope systems can be written as Eq. (3).

$$q_u = f(B.X.u.h.\theta.L.D_r.D_{50}.\phi.c.\gamma.\upsilon.E_{soil}.E_{geo}.b) \quad (3)$$

The equation comprises 15 parameters which two of them have fundamental dimensions (i.e. length and force). So, Eq. (3) can be reduced to 13 non-dimensional parameters and substituted with Eq. (4).

$$\frac{q_u}{\gamma B} = f\left(\frac{x}{B}.\frac{u}{B}.\frac{h}{B}.\theta.\frac{L}{x}.D_r.\frac{D_{50}}{B}.\frac{c}{\gamma B}.\frac{\gamma D_{50}}{E_{soil}}.\upsilon.\frac{E_{soil}}{E_{geo}}.\frac{b}{D_{50}}\right) \quad (4)$$

For a prototype footing (p) with diameter n times of that in the model (m), Eq. (5) can be considered.

$$\frac{B_P}{B_m} = n \quad (5)$$

For similarity to be maintained, all the non-dimensional terms in both model and prototype need to be equal. As an

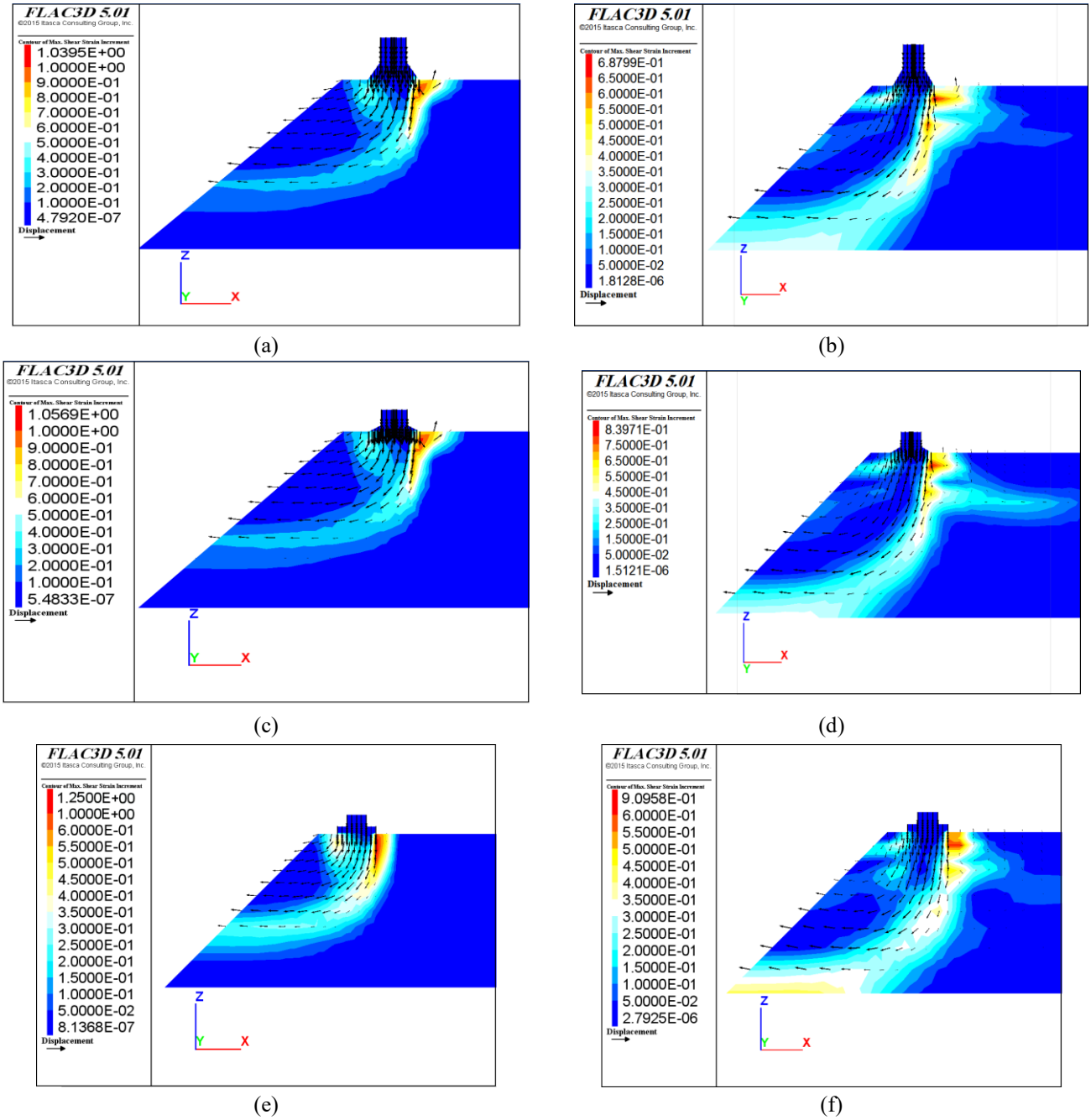

Fig. 19 Shear strain contours for footings with (a, b) i=60°, (c, d) i=120°, (e, f) i=180° (left side for unreinforced and right side for reinforced slopes)

example, if a strip footing with width of 140 cm is assumed therefore, it means n=10 and parameters X, u, h, L, D_{50} and b should be considered 10 times of the model parameters. Assuming that the soils used in the model and prototype do have the same unit weight, then parameters, including c, E_{soil} and E_{geo} should also be considered 10 times of the model parameters, as well.

In this situation, Eq. (6) can be satisfied to obtain the bearing capacity of prototype system.

$$\left(\frac{q_u}{\gamma B}\right)_m = \left(\frac{q_u}{\gamma B}\right)_p \xrightarrow{\text{yields}} (q_u)_p = n(q_u)_m \qquad (6)$$

In order to assess the proposed scaling rules and also, to investigate the bearing capacity of large scale shell footings located at the slope surface, the scale factor "n" is assumed to be 5 and 10. Therefore, according to Eq. (4), the geometric dimensions of the reinforced slopes and footings are considered 5 and 10 times of the model parameters. Then, analyses were carried out until the footings' settlement approached to 10% of the corresponding footings' width.

Fig. 21 shows the stress-settlement curves for reinforced slopes considering the scale factor of 5 and 10 for shell footings with different peak angle (i=60° and i=120°) as

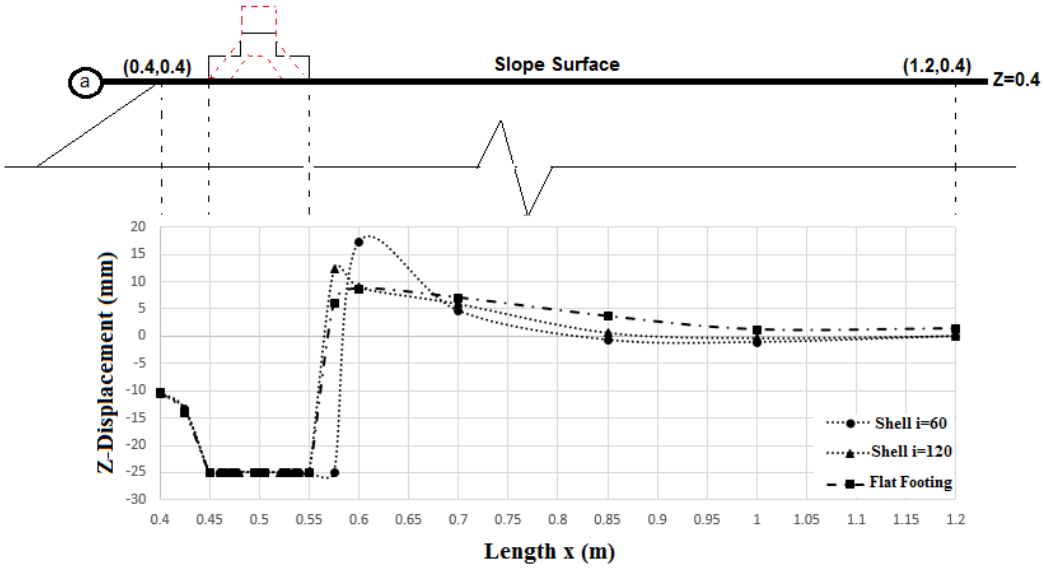

Fig. 20 Comparison of vertical displacements at the ground surface for all footings in unreinforced status

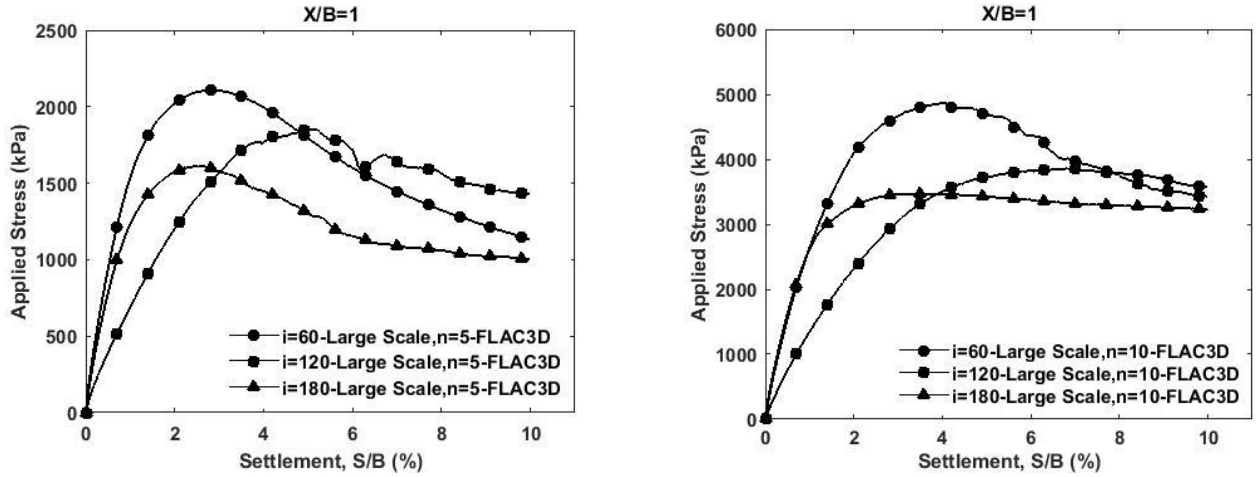

(a) (b)

Fig. 21 Response of the shell footings with apex angle of 60° at edge distance X=1B for slope angles of 30°, 45°, 60°, and plane backfill under the applied force for (a) unreinforced, and (b) reinforced embankment

Table 7 Comparison of the bearing capacity of reinforced slopes for the scale factors of 5, and 10

		Maximum stress Failure (kPa)		$n = \frac{(q_u)_p}{(q_u)_m}$
		$(q_u)_p$	$(q_u)_m$	
Large Scale n=5	Shell i=60	540.77	2107.56	3.89
	Shell i=120	411.07	1852.95	4.50
	Flat Footing	375.70	1611.88	4.29
Large Scale n=10	Shell i=60	540.77	4866.42	8.99
	Shell i=120	411.07	3857.14	9.38
	Flat Footing	375.70	3469.64	9.30

well as flat footing (i=180°). Table 7 compares the bearing capacity of footings for the reinforced slopes for the scale factors of 5, and 10.

According to Table 7, bearing capacity of footings on large scale reinforced slopes with scale factors of 5, and 10, were obtained approximately 4.2 and 9.2 times of small scale model (the basic model). It indicates that the proposed scaling rule represented by Tavakoli Mehrjardi *et al*. (2016) has good accuracy to small scale model and therefore, it can be applied to convert the obtained results in small scale model to prototype models. It should be noted that the above-mentioned dimensional analysis is limited for elastic response of reinforcements. Otherwise, for nonlinear behaviour of reinforcements and depending on the transferred stress level in geotextiles, the relationships should be fully justified.

6. Conclusions

A series of numerical simulations verifying with reduced scale physical modelling was carried out to study the performance of shell strip footings placed on the unreiforced and reinforced slopes. As a whole, this study exhibited further studies to understand the stress distribution in the backfill beneath the shell footings in comparison with flat footings. Moreover, the interpretation of the obtained results for prototype problems (scale effect), influence of contributory factors such as the core in shell footings, stiffness of shell footing materials, and slope angle, which cannot be not easily achievable using experimental models, were discussed in this paper.

Therefore, the results can lay groundwork for design and practice. The following results can be itemized:

- With decreasing the apex angle from 180° to 60°, the bearing capacity climbed drastically irrespective of reinforcement status and edge distance.
- The shell footing with apex angle 60° has owned larger contact area with soil through the core in comparison with the other types of footings, leading to propagation of the lower vertical stress in the backfill.
- Vertical stress level in shell foundations is about 50% to 75% of that in flat foundation. In effect, the core plays a key role in stress reduction.
- The depth of the failure wedge for shell footings with apex angle of 60°, 120° and 180° were about 0.5B, 0.4B, and 0.1B, respectively. It means that more passive forces were provided against the footing penetration, bringing about higher bearing capacity for this kind of footing.
- The safe edge distance for shell footing with apex angle of 60° was 2B, while that for flat footing was about 4B. This confirms that shell footings over the slope surface are more reliable in contrast with conventional flat footings.
- In unreinforced slopes, the most optimal edge distance and apex angle were 1.8 and 60°, respectively. In reinforced slope, these values were 1 and 60°, achieving the least ultimate bearing capacity which reflected IF>1.
- Regardless of apex angle, shell's core made of dense soil obtained the highest bearing capacity among the other materials. In fact, erecting the shell footings with no material (air) caused stress concentration beneath the footings bases which, in turn, gave rise to the weakest response of the foundations.
- In unreinforced slopes, the most optimal slop angle and apex angle were 39° and 60°, respectively. In reinforced slope, these values are 50° and 60°, achieving the least ultimate bearing capacity which reflected IF>1.
- Irrespective of the reinforcement conditions, the bearing capacity of flat footings were smaller owing to the fact that the shear strains, propagated beneath the footing, were larger which it confirms the lower efficiency of these footings in contrast with shell footings.
- Bearing capacity of footings on large scale reinforced slopes with different scale factors was investigated based on the proposed scaling rule represented by Tavakoli Mehrjardi *et al*. (2016). It can be successfully applied to convert the obtained results from small scale model to prototype models.

References

Azzam, W.R. and Nasr, A.M. (2015), "Bearing capacity of shell strip footing on reinforced sand", *J. Adv. Res.*, **6**(5), 727-737. https://doi.org/10.1016/j.jare.2014.04.003.

Borthakur, B.C., Nambiar, M.K.C., Biswas, A. and Kalitha, U.C. (1988), "Studies on the bearing capacity of strip footing on slopes". *Proceedings of the Indian Geotechnical Conference.*, Bombay, India.

Cardile, G., Moraci, N. and Pisano, M., (2017), "Tensile behaviour of an HDPE geogrid under cyclic loading: experimental results and empirical modelling", *Geosynth. Int*., **24**, 95-112. https://doi.org/10.1680/jgein.16.00019.

El-kady, M. and Badrawi, E. (2017), "Performance of isolated and folded footings", *J. Comput. Des. Eng.*, **4**(2), 150-157. https://doi.org/10.1016/j.jcde.2016.09.001.

Esmaili D. and Hataf N., (2008), "Experimental and numerical investigation of ultimate load capacity of shell foundations on reinforced and unreinforced sand", *Iranian J. Sci. Tech*., **32**, 491-500.

Ferreira, F.B., Topa Gomes, A., Vieira, C.S. and Lopes, M.L. (2016), "Reliability analysis of geosynthetic-reinforced steep slopes", *Geosynth. Int.*, **23**(4), 301-315. https://doi.org/10.1680/jgein.15.00057.

Grant, F. (2007), Design Expert 7.1., Scientific Computing World.

Ghaffari, S.A., Hamidi, A. and Tavaloli Mehrjardi, Gh. (2021), "Bearing capacity of triangular shell foundations adjacent to the reinforced sandy slopes", *Eng. Geol*., **14**(5), 1-36. https://doi.org/10.52547/jeg.14.5.1.

Ghaffari, S.A., Sattari, E., Hamidi, A., Tavaloli Mehrjardi, Gh., and Homayoun Rooz, A.F. (2021), "Experimental study on bearing capacity of shell strip footings near geotextile-reinforced earth slopes", *J. Cent. South Univ*., **28**, 2527-2543. https://doi.org/10.1007/s11771-021-4784-9.

Hanna, A. and Abdel-Rahman, M. (1990), "Ultimate bearing capacity of triangular shell strip footings on sand", *J. Geotech. Eng. - ASCE*, **116**(12), 1851-1863. https://doi.org/10.1061/(ASCE)0733-9410.

Hanna, A. and Abdel-Rahman, M. (1998), "Experimental investigation of shell foundations on dry sand", *Can. Geotech. J.*, **35**(5), 847-857. https://doi.org/10.1139/cgj-35-5-847.

Hussaini, S.K., Indraratna, B. and Vinod, J.S. (2015), "Performance assessment of geogrid-reinforced railroad ballast during cyclic loading", *Transport. Geotech.*, **2**(6), 99-107. https://doi.org/10.1016/j.trgeo.2014.11.002.

Indraratna, B., Hussaini, S.K.K. and Vinod, J.S. (2013), "The lateral displacement response of geogrid-reinforced ballast under cyclic loading", *Geotext. Geomembranes*, **39**(3), 20-29. https://doi.org/10.1016/j.geotexmem.2013.07.007.

Itasca. (2011), "Fast Lagrangian analysis of continua in 3 dimensions", user's guide, FLAC 3D V5.0., Minneapolis, Itasca Consulting Group.

Iyer, T.S. and Rao, N.R. (1970), "Model studies on funicular shells as rafts on sands", *Proceedings of the symposium on shallow foundations,* Bombay, India.

Javankhoshdel, S. and Bathurst, R.J. (2016), "Influence of cross correlation between soil parameters on probability of failure of simple cohesive and c-f slopes", *Can. Geotech. J.*, **53**(5), 839-853. https://doi.org/10.1139/cgj-2015-0109.

Kurian, N.P. (1994), "Behaviour of shell foundations under subsidence of core Soil", *Proceedings of the 13th International Conference on Soil Mechanics and Foundation Engineering*, New Delhi, India, 5 - 10 January.

Kurian, N.P. and Mohan, C.S. (1983), "Ultimate strength of hyperbolic parabolic shell foundations under vertical loads and moments", *Bull. Int. Assoc. Shel Spatial Struct*., **24-1**(81), 27-42.

Kurian, N.P. and Mohan, C.S. (1981), "Contact pressures under shell foundations", *Proceedings of the 10th International Conference on Soil Mechanics and Foundation Engineering*, Stockholm, Sweden.

Tavaloli Mehrjardi, Gh., Behrad, R. and Tafreshi, S.N. (2019), "Scale effect on the behavior of geocell-reinforced soil", *Geotext. Geomembranes*, **47**(2), 154-163. https://doi.org/10.1016/J.GEOTEXMEM.2018.12.003.

Tavaloli Mehrjardi, Gh., Ghanbari, A. and Mehdizadeh, H., (2016), "Experimental study on the behaviour of geogrid-reinforced slopes with respect to aggregate size", *Geotext. Geomembranes*, **44**(6), 862-871. https://doi.org/10.1016/j.geotexmem.2016.06.006.

Tavaloli Mehrjardi, Gh. and Khazaei, M. (2017), "Scale effect on the behaviour of geogrid-reinforced soil under repeated loads", *Geotext. Geomembranes,* **45**(6), 603-615. https://doi.org/10.1016/j.geotexmem.2017.08.002.

Meyerhof, G.G. (1957), "The ultimate bearing capacity of foundation on slopes", *Proceedings of the 4th International Conference on Soil Mechanics and Foundation Engineering*.

Moghaddas Tafreshi, S.N., Joz Darabi, N., Tavaloli Mehrjardi, Gh. and Dawson, A. (2016), "Experimental and numerical investigation of footing behaviour on multi-layered rubber-reinforced soil", *Eur. J. Environ. Civil Eng.*, **23**(1), 29-–52. https://doi.org/10.1080/19648189.2016.1262288.

Moghaddas Tafreshi S.N., Shaghaghi T., Tavaloli Mehrjardi, Gh., Dawson A. and Ghadrdan M., (2015), "A simplified method for predicting the settlement of circular footings on multi-layered geocell-reinforced non-cohesive soils", *Geotextiles and Geomembranes.*, **43**(4), 332-344. https://doi.org/10.1016/j.geotexmem.2015.04.006.

Shaligram, P.S. (2011), "Behaviour of triangular shell strip footing on georeinforced layered sand", *Int. J. Adv. Eng. Tech.*, **2**, 192-196.

Shields, D.H., Scott, J.D., Bauer, G.E., Deschemes, J.H. and Barsvary, A.K., (1977), "Bearing capacity of foundations near slopes", *Proceedings of the 9th International Conference on Soil Mechanics and Foundation Engineering*.

Suku, L., Prabhu, S.S. and Sivakumar Babu, G.L. (2017), "Effect of geogrid-reinforcement in granular bases under repeated loading", *Geotext. Geomembranes*, **45**(4), 377-389. https://doi.org/10.1016/j.geotexmem.2017.04.008.

CC